J. Fluid Mech. (2004), *vol.* 501, *pp.* 1–24. © 2004 Cambridge University Press
DOI: 10.1017/S0022112003006220 Printed in the United Kingdom

Translational motion of a bubble undergoing shape oscillations

By ALEXANDER A. DOINIKOV

Institute of Nuclear Problems, Belarus State University, 11 Bobruiskaya Street, Minsk 220050, Belarus
doinikov@inp.minsk.by

(Received 15 April 2002 and in revised form 19 June 2003)

This paper studies the nonlinear coupling between the volume pulsation, translational motion and shape modes of an oscillating bubble, especially in the context of translational instability, known as 'dancing motion', that is demonstrated by bubbles in acoustic standing waves. A set of coupled equations is derived that describes volume pulsations of a bubble, its translational motion and shape oscillations evolving on the bubble surface. The amplitudes of the surface modes and the translational velocity of the bubble are assumed to be small and allowed for in the equations of motion up to only second-order terms. The amplitude of the volume oscillation is not limited. Unlike earlier work on this subject, where only two adjacent shape modes with given natural frequencies are taken into account, we allow for all shape modes and do not impose any limitations on their natural frequencies. As a result, the present analysis reveals additional features, which have not been noted previously, inherent in the mutual interactions of the shape modes as well as in the interaction between the shape modes and the translational motion.

1. Introduction

When a gas bubble in a liquid is subjected to a standing acoustic wave, it moves towards either the pressure node or the pressure antinode, depending on the relation between its resonant (Minnaert) frequency and the driving frequency of the acoustic field, and is held there as long as the sound is on. This effect is explicable on the basis of the well-known formula, derived by Eller (1968), which gives the so-called primary Bjerknes force experienced by a spherical bubble in a standing sound wave. However, the bubble behaviour described occurs only in relatively weak acoustic fields. When the acoustic pressure amplitude exceeds a threshold value, the trapped bubble begins an erratic motion called 'dancing motion'. This curious phenomenon was first noticed by Gaines (1932) and has been reported by many others ever since (Kornfeld & Suvorov 1944; Benjamin & Strasberg 1958; Strasberg & Benjamin 1958; Benjamin 1964; Eller & Crum 1970).

Benjamin & Strasberg (1958; see also Benjamin 1964) suggested that the erratic dancing motion of a bubble trapped in a standing acoustic wave is caused by the presence of shape oscillations that are parametrically excited by the bubble pulsations. In an attempt to verify this suggestion, they compared measured thresholds for the onset of dancing to calculated thresholds for the onset of shape oscillations. Oversimplifications in their theoretical approach, however, prevented adequate agreement of theory with experiment. Several years later, a similar study was made by Eller & Crum (1970), who applied a more accurate method of calculation and in

https://doi.org/10.1017/S0022112003006220 Published online by Cambridge University Press

consequence obtained good agreement between the measured dancing thresholds and the calculated shape-oscillation thresholds. It has since been universally recognized that the dancing bubble motion in sound fields is caused by parametrically excited shape oscillations.

The next step in revealing mechanisms responsible for the bubble dancing was made by Benjamin & Ellis (1990). Using a relevant theory developed by Benjamin (1987) in an earlier paper, they derived a formula for the drift velocity of an oscillating bubble from which it follows that the translational motion of the bubble can result from second-order interactions between two neighbouring surface deformation modes. However, the above formula allows us to calculate explicitly the drift velocity only when the motions of surface modes are known.

The results of Benjamin & Ellis (1990) have since been used by Mei & Zhou (1991). In an attempt to explain the dancing motion of a bubble in a sound field, they studied the nonlinear resonance between the volume oscillations and two adjacent shape modes of a bubble. In particular, they derived amplitude equations governing the dynamics of these three modes and showed that the resonant interactions could lead to chaotic oscillations of the shape modes and thus erratic drift according to the formula obtained by Benjamin & Ellis. The theory of Mei & Zhou is, however, incomplete as it assumes that there is no direct coupling between the translational motion of the bubble and the dynamics of the shape modes.

Development of an adequate model of the bubble dancing requires consideration of the coupling between translational motion, volume oscillations and surface modes. An attempt to allow for this coupling has been made by Feng & Leal (1995). They have derived coupled amplitude equations that govern the dynamics of the bubble centroid, as well as volume oscillations and two adjacent shape modes. In doing so, unlike Mei & Zhou, Feng & Leal did not assume the volume mode to be in resonance with the isotropic pressure forcing. Their study verified that the instability of two neighbouring shape modes results in a translational motion of the bubble.

As in the work of Feng & Leal (1995), the purpose of the present study is to derive coupled equations that govern the volume oscillations of an acoustically driven bubble, its translational motion and the shape modes evolving on the bubble surface. These equations are then solved numerically to examine conditions when the bubble exhibits a translational instability. Like Feng & Leal, we apply a perturbation analysis, where the amplitudes of the shape modes and the translational velocity of the bubble are small parameters, and derive the above-mentioned equations of motion with accuracy up to quadratic terms in those quantities. Unlike Feng & Leal, who deal only with two adjacent shape modes whose natural frequencies are taken to be approximately equal to half the driving frequency, we allow for all shape modes and do not impose any limitations on their natural frequencies. In the present analysis, we also take into account that the shape modes can be excited not only parametrically by the volume oscillations, but also through variations of the sound pressure over the surface of the bubble.

2. Theory

Let us consider a gas bubble in an infinite incompressible inviscid liquid subject to an acoustic wave field. For simplicity, we assume that deformations of the bubble surface are axisymmetric and the translational motion of the bubble occurs along the axis of symmetry. In practice, translations of bubbles in sound fields have, of course, three spatial components. The theory developed in this study can, in principle, be

https://doi.org/10.1017/S0022112003006220 Published online by Cambridge University Press

extended to arbitrary asymmetric perturbations. However, the algebraic complexity involved and the unwieldiness of the resulting expressions prevent us from carrying out such an analysis in the present paper. We also expect that, if the forcing is axisymmetric, as in the case of a plane standing wave considered here, axisymmetric modes are dominant. Although taking account of asymmetric modes brings the analysis closer to reality, it is improbable that something fundamentally new, from the theoretical standpoint, will emerge as compared to the axisymmetric case. So we assume that the perturbed surface S of the bubble is described by the equation

$$S(r,\theta,t) = r - R(t) - \sum_{n=2}^{\infty} s_n(t) P_n(\mu) = 0, \tag{2.1}$$

where r and θ are spherical coordinates in a coordinate system whose origin coincides with the bubble centroid, t is time, $R(t)$ is the bubble radius, $\mu = \cos\theta$, P_n is the Legendre polynomial of order n, and $s_n(t)$ are the amplitudes of the shape modes. Recall that, like Feng & Leal (1995), we seek to derive coupled equations that govern the dynamics of the bubble volume, the translational motion and the shape modes, correct to quadratic terms in the amplitudes of the shape modes and the translational velocity of the bubble, assuming these quantities to be small. No restrictions are imposed on the volume oscillations which are defined by $R(t)$.

The velocity potential in the liquid, which should satisfy the Laplace equation, can be written as

$$\varphi = -\frac{R^2(t)\dot{R}(t)}{r} + \sum_{n=0}^{\infty} \frac{a_n(t)}{r^{n+1}} P_n(\mu), \tag{2.2}$$

where the overdot denotes the time derivative and the coefficients $a_n(t)$, which, like $s_n(t)$, are assumed to be small, are determined by the boundary conditions at the bubble surface. The liquid velocity is found from (2.2) to be

$$\boldsymbol{v} = \nabla\varphi = \frac{R^2(t)\dot{R}(t)}{r^2}\boldsymbol{e}_r - \sum_{n=0}^{\infty} \frac{a_n(t)}{r^{n+2}} [(n+1)P_n(\mu)\boldsymbol{e}_r + \sin\theta\, P_n'(\mu)\boldsymbol{e}_\theta], \tag{2.3}$$

where $P_n'(\mu) = \mathrm{d}P_n(\mu)/\mathrm{d}\mu$. To obtain equations that govern the dynamics of $s_n(t)$ and $a_n(t)$, we first use the kinematic boundary condition

$$\frac{\partial S}{\partial t} - \boldsymbol{u}\cdot\nabla S + \boldsymbol{v}\cdot\nabla S = 0 \quad \text{on } S, \tag{2.4}$$

where $\boldsymbol{u}(t)$ denotes the translational velocity of the bubble. Recall that this velocity is considered to be a small quantity. From (2.1), we find

$$\frac{\partial S}{\partial t} = -\dot{R}(t) - \sum_{n=2}^{\infty} \dot{s}_n(t) P_n(\mu), \tag{2.5}$$

$$\nabla S|_S \approx \boldsymbol{e}_r + \frac{\boldsymbol{e}_\theta \sin\theta}{R(t)} \sum_{n=2}^{\infty} s_n(t) P_n'(\mu). \tag{2.6}$$

Note that although (2.6) gives ∇S only up to linear terms, this is, as evident from (2.4), quite enough for our analysis.

https://doi.org/10.1017/S0022112003006220 Published online by Cambridge University Press

The liquid velocity $\boldsymbol{v}$ on the bubble surface S, with accuracy up to second-order terms, is given by

$$\boldsymbol{v}|_S \approx \frac{\dot{R}\boldsymbol{e}_r}{R^2}\left[R^2 - \sum_{n=2}^{\infty} s_n\left(2R - 3\sum_{m=2}^{\infty} s_m P_m\right)P_n\right] - \sum_{n=0}^{\infty}\frac{a_n}{R^{n+2}}\left(1 - \frac{n+2}{R}\sum_{m=2}^{\infty} s_m P_m\right)[(n+1)P_n\boldsymbol{e}_r + \sin\theta P_n'\boldsymbol{e}_\theta], \quad (2.7)$$

where the dependence on t and μ is omitted for the sake of simplicity. Substituting (2.5)–(2.7) into (2.4), we obtain

$$R^2 a_0 + (2a_1 R + R^4 u)\mu + \sum_{n=2}^{\infty}\left(R^4\dot{s}_n + 2\dot{R}R^3 s_n + \frac{(n+1)a_n}{R^{n-2}}\right)P_n = \sum_{n=2}^{\infty}\left\{2(Ra_0 + 3a_1\mu)s_n P_n + (R^3 u - a_1)(1-\mu^2)s_n P_n' + \sum_{m=2}^{\infty}\left[\left(3\dot{R}R^2 s_n s_m + \frac{(m+1)(m+2)s_n a_m}{R^{m-1}}\right)P_n P_m - \frac{s_n a_m}{R^{m-1}}(1-\mu^2)P_n' P_m'\right]\right\} \quad (2.8)$$

with $\boldsymbol{u} = |\boldsymbol{u}(t)|$. To proceed, we need expansions of $\mu P_n(\mu)$, $(1-\mu^2)P_n'(\mu)$, $P_n(\mu)P_m(\mu)$ and $(1-\mu^2)P_n'(\mu)P_m'(\mu)$ in terms of the Legendre polynomials. The expansions of the first two products are familiar (Abramowitz & Stegun 1972):

$$\mu P_n(\mu) = \frac{nP_{n-1}(\mu) + (n+1)P_{n+1}(\mu)}{2n+1}, \quad (1-\mu^2)P_n'(\mu) = \frac{n(n+1)}{2n+1}[P_{n-1}(\mu) - P_{n+1}(\mu)]. \quad (2.9)$$

The other two expressions are found by using the so-called Clebsch–Gordan expansion (Varshalovich, Moskalev & Khersonskii 1975). The result is as follows:

$$P_n(\mu)P_m(\mu) = \sum_{l=0}^{\infty} C_l(n,m)P_l(\mu), \quad (1-\mu^2)P_n'(\mu)P_m'(\mu) = \sum_{l=0}^{\infty} D_l(n,m)P_l(\mu). \quad (2.10)$$

The coefficients $C_l(n,m)$ are determined by

$$C_l(n,m) = (nm00\,|\,nml0)^2, \quad (2.11)$$

where $(nm00\,|\,nml0)$ denotes the Clebsch–Gordan coefficients as defined in Abramowitz & Stegun (1972). For the coefficients $D_l(n,m)$, we have

$$D_l(n,m) = \frac{n(n+1)}{2n+1}\sum_{k=1}^{M}(2m-4k+3)[C_l(n-1,m-2k+1) - C_l(n+1,m-2k+1)], \quad (2.12)$$

where $M = m/2$ for even values of m, and $M = (m+1)/2$ for odd values of m. Note also that the following identities are valid, which follow from the symmetry of the left-hand sides of equations (2.10) with respect to the indices n and m,

$$C_l(n,m) = C_l(m,n), \quad D_l(n,m) = D_l(m,n). \quad (2.13a)$$

https://doi.org/10.1017/S0022112003006220 Published online by Cambridge University Press

The properties of the Clebsch–Gordan coefficients also give

$$C_l(n,m) = \frac{2l+1}{2n+1} C_n(l,n) = \frac{2l+1}{2m+1} C_m(n,l). \tag{2.13b}$$

These identities make the explicit calculation of the coefficients $C_l(n,m)$ and $D_l(n,m)$ much easier. It should be pointed out that we have used here a simplified (axisymmetric) form of the Clebsch–Gordan expansion. Turning back to the assumption of axial symmetry, if we wish to extend the present analysis to asymmetric perturbations, the Legendre polynomials in the foregoing calculation should be changed to spherical harmonics and the general form of the Clebsch–Gordan expansion should then be applied. However, as mentioned above, this results in very cumbersome equations.

Substituting (2.9) and (2.10) into (2.8) and equating quantities at the same Legendre polynomials, we find

$$a_0(t) = H_0(t), \quad a_1(t) = -\tfrac{1}{2}R^3 u + \tfrac{3}{10}R^2 s_2 u + H_1(t), \tag{2.14}$$

$$a_n(t) = -\frac{R^{n+1}}{n+1}[2s_n\dot{R} + \dot{s}_n R] + \frac{3nR^{n+1}u}{2}\left[\frac{s_{n+1}}{2n+3} - \frac{(1-\delta_{2n})s_{n-1}}{2n-1}\right] + H_n(t), \quad n \geqslant 2, \tag{2.15}$$

where

$$H_n(t) = \frac{R^n}{n+1}\sum_{l,m=2}^{\infty}\left\{\dot{R}\left[\frac{2D_n(l,m)}{(l+1)} - (2l+1)C_n(l,m)\right]s_l s_m + R\left[\frac{D_n(l,m)}{(l+1)} - (l+2)C_n(l,m)\right]\dot{s}_l s_m\right\} \tag{2.16}$$

and δ_{2n} is the Kronecker delta.

The next step is the use of the normal stress boundary condition

$$p_g = p|_S + p_{st} + p_{ex}|_S, \tag{2.17}$$

where p_g is the pressure of the gas within the bubble, $p|_S$ is the pressure in the liquid at the bubble surface, p_{st} is the pressure of surface tension, and $p_{ex}|_S$ is the external (acoustic) pressure acting on the bubble. The gas pressure is assumed to obey the adiabatic law

$$p_g = P_{g0}\left(\frac{V_0}{V(t)}\right)^{\gamma}, \tag{2.18}$$

where $P_{g0} = P_0 + 2\sigma/R_0$ is the equilibrium gas pressure, P_0 is the hydrostatic pressure in the liquid, σ is the surface tension coefficient, R_0 is the equilibrium bubble radius, $V_0 = (4/3)\pi R_0^3$ is the equilibrium bubble volume, $V(t)$ is the instantaneous bubble volume, and γ is the ratio of specific heats of the gas. Correct to second order, the gas pressure is found to be

$$p_g \approx P_{g0}\left(\frac{R_0}{R}\right)^{3\gamma}\left(1 - \frac{3\gamma}{R^2}\sum_{m=2}^{\infty}\frac{s_m^2}{2m+1}\right). \tag{2.19}$$

The pressure in the liquid is specified by

$$p|_S = P_0 - \rho\left(\frac{\partial\varphi}{\partial t} - \boldsymbol{u}\cdot\boldsymbol{v} + \frac{v^2}{2}\right)_S, \tag{2.20}$$

where ρ denotes the density of the liquid. The explicit expression for $p|_S$, accurate to second-order terms, is not given here because of its unwieldiness. The pressure of

https://doi.org/10.1017/S0022112003006220 Published online by Cambridge University Press

surface tension, assuming that σ is small, can be written as (Prosperetti 1977)

$$p_{st} = \sigma \nabla \cdot \boldsymbol{n} \approx \frac{2\sigma}{R} + \frac{\sigma}{R^2} \sum_{n=2}^{\infty} (n-1)(n+2) s_n P_n(\mu), \tag{2.21}$$

where $\boldsymbol{n}$ is the outward unit normal to S. Finally, the external pressure is represented by

$$p_{ex}|_S = \sum_{n=0}^{\infty} A_n(t) P_n(\mu), \tag{2.22}$$

where the coefficients $A_n(t)$ are determined by the type of incident field. In Appendix A, they are calculated for the case of a plane standing wave, which will be analysed below in this paper.

Substituting (2.19)–(2.22) into (2.17), using (2.9), (2.10), (2.14)–(2.16) and then equating quantities at the same Legendre polynomials, we obtain a set of coupled equations that govern the dynamics of the volume oscillations, translational motion and shape modes, with accuracy up to second-order terms in s_n,

$$R\ddot{R} + \tfrac{3}{2}\dot{R}^2 = \frac{1}{\rho}\left[P_{g0}\left(\frac{R_0}{R}\right)^{3\gamma} - \frac{2\sigma}{R} - P_0 - A_0\right] + \frac{u^2}{4} + f_0(t), \tag{2.23}$$

$$\left(R - \tfrac{7}{5}s_2\right)\dot{u} + \left(3\dot{R} - \frac{12\dot{R}}{5R}s_2 - \tfrac{9}{5}\dot{s}_2\right)u = -\frac{2}{\rho}A_1 + f_1(t), \tag{2.24}$$

$$R\ddot{s}_n + 3\dot{R}\dot{s}_n + \left[\frac{(n^2-1)(n+2)\sigma}{\rho R^2} - (n-1)\ddot{R}\right]s_n = -\frac{n+1}{\rho}A_n - \frac{9\delta_{2n}}{4}u^2 + g_n(t) + f_n(t), \quad n \geqslant 2, \tag{2.25}$$

where

$$f_n(t) = -\frac{3\gamma P_{g0} R_0^{3\gamma}\delta_{n0}}{\rho R^{3\gamma+2}} \sum_{l=2}^{\infty} \frac{s_l^2}{2l+1} + \sum_{l,m=2}^{\infty} s_l s_m \left[\frac{\ddot{R}}{R}\alpha_1(n,l,m) + \frac{\dot{R}^2}{R^2}\alpha_2(n,l,m)\right] + \alpha_3(n,l,m)\ddot{s}_l s_m + \alpha_4(n,l,m)\frac{\dot{R}}{R}(\dot{s}_l s_m + \dot{s}_m s_l) + \alpha_5(n,l,m)\dot{s}_l\dot{s}_m, \tag{2.26}$$

$$g_n(t) = \frac{n+1}{2(2n+3)}\left[6(n+1)\frac{\dot{R}}{R}s_{n+1}u + (5n+2)s_{n+1}\dot{u} + 3(2n+1)\dot{s}_{n+1}u\right] - \frac{(n+1)(1-\delta_{2n})}{2(2n-1)}\left[6(n-1)\frac{\dot{R}}{R}s_{n-1}u + n s_{n-1}\dot{u} + 3(2n-1)\dot{s}_{n-1}u\right], \tag{2.27}$$

$$\alpha_1(n,l,m) = \frac{2D_n(l,m)}{m+1} - (2l-n)C_n(l,m), \tag{2.28}$$

$$\alpha_2(n,l,m) = (2l-n)C_n(l,m) - \frac{2(l-n)D_n(l,m)}{(l+1)(m+1)}, \tag{2.29}$$

$$\alpha_3(n,l,m) = \frac{D_n(l,m)}{l+1} - (l-n+1)C_n(l,m), \tag{2.30}$$

https://doi.org/10.1017/S0022112003006220 Published online by Cambridge University Press

$$\alpha_4(n,l,m) = \frac{(2l+n+3)D_n(l,m)}{(l+1)(m+1)} - (2l-n)C_n(l,m), \tag{2.31}$$

$$\alpha_5(n,l,m) = \frac{(2l+n+3)D_n(l,m)}{2(l+1)(m+1)} - \tfrac{1}{2}(2l-n+3)C_n(l,m). \tag{2.32}$$

In these equations, for simplicity, the dependence on t in the functions that we have already met is omitted. Equation (2.23) governs the volume oscillation of the bubble, (2.24) its translational motion, and (2.25) the dynamics of the shape modes. All the equations are coupled owing to the functions $f_n(t)$ and $g_n(t)$, as well as the presence of the term u^2 on the right-hand sides of (2.23) and (2.25). Note also that although the translational velocity u was assumed here to be small, (2.23) and (2.24) are valid for arbitrary values of u. This follows from comparison of these equations with similar equations which were obtained earlier (except, of course, for the shape-mode terms), not restricting the magnitude of the translational velocity (Kuznetsov & Shchekin 1973; Harkin, Kaper & Nadim 2001). In the next section, we shall restrict our consideration to the first three shape modes, neglecting in (2.23)–(2.27) all the modes higher than s_4. The truncated equations are more amenable to analysis since they allow us to see the real structure of the functions $f_n(t)$.

3. Equations accurate to the fourth mode

When (2.23)–(2.27) are taken with accuracy up to the fourth shape mode s_4, we obtain the following set of equations:

$$R\ddot{R} + \tfrac{3}{2}\dot{R}^2 = \frac{1}{\rho}\left[P_{g0}\left(\frac{R_0}{R}\right)^{3\gamma} - \frac{2\sigma}{R} - P_0 - A_0 - \frac{4\eta\dot{R}}{R}\right] + \frac{u^2}{4} + f_0^{(4)}(t), \tag{3.1}$$

$$\left(R - \tfrac{7}{5}s_2\right)\dot{u} + \left(3\dot{R} - \frac{12\dot{R}}{5R}s_2 - \tfrac{9}{5}\dot{s}_2\right)u = -\frac{2}{\rho}A_1 + f_1^{(4)}(t) - \frac{18\eta u}{\rho R}, \tag{3.2}$$

$$R\ddot{s}_2 + 3\dot{R}\dot{s}_2 + \left(\frac{12\sigma}{\rho R^2} - \ddot{R}\right)s_2 = -\frac{3}{\rho}A_2 - \tfrac{9}{4}u^2 + f_2^{(4)}(t) + g_2^{(4)}(t), \tag{3.3}$$

$$R\ddot{s}_3 + 3\dot{R}\dot{s}_3 + \left(\frac{40\sigma}{\rho R^2} - 2\ddot{R}\right)s_3 = -\frac{4}{\rho}A_3 + f_3^{(4)}(t) + g_3^{(4)}(t), \tag{3.4}$$

$$R\ddot{s}_4 + 3\dot{R}\dot{s}_4 + \left(\frac{90\sigma}{\rho R^2} - 3\ddot{R}\right)s_4 = -\frac{5}{\rho}A_4 + f_4^{(4)}(t) + g_4^{(4)}(t), \tag{3.5}$$

where

$$\begin{aligned} f_0^{(4)}(t) = {} & \frac{1}{30}\left(\frac{8\dot{R}^2}{R^2}s_2^2 - 6s_2\ddot{s}_2 + \frac{8\dot{R}}{R}s_2\dot{s}_2 - 7\dot{s}_2^2\right) \\ & + \frac{1}{56}\left(\frac{12\dot{R}^2}{R^2}s_3^2 - 8s_3\ddot{s}_3 + \frac{12\dot{R}}{R}s_3\dot{s}_3 - 9\dot{s}_3^2\right) \\ & + \frac{1}{90}\left(\frac{16\dot{R}^2}{R^2}s_4^2 - 10s_4\ddot{s}_4 + \frac{16\dot{R}}{R}s_4\dot{s}_4 - 11\dot{s}_4^2\right) \\ & - \frac{3\gamma P_{g0}R_0^{3\gamma}}{\rho R^{3\gamma+2}}\left(\frac{s_2^2}{5} + \frac{s_3^2}{7} + \frac{s_4^2}{9}\right), \end{aligned} \tag{3.6}$$

https://doi.org/10.1017/S0022112003006220 Published online by Cambridge University Press

$$f_1^{(4)}(t) = \frac{3}{35}\left[4\left(\frac{\ddot{R}}{R} + \frac{3\dot{R}^2}{R^2}\right)s_2 s_3 + 2\ddot{s}_2 s_3 - 3s_2\ddot{s}_3 + \frac{12\dot{R}}{R}(\dot{s}_2 s_3 + s_2\dot{s}_3) - 3\dot{s}_2\dot{s}_3\right]$$
$$+ \frac{1}{21}\left[6\left(\frac{\ddot{R}}{R} + \frac{3\dot{R}^2}{R^2}\right)s_3 s_4 + 3\ddot{s}_3 s_4 - 4s_3\ddot{s}_4 + \frac{18\dot{R}}{R}(\dot{s}_3 s_4 + s_3\dot{s}_4) - 3\dot{s}_3\dot{s}_4\right], \quad (3.7)$$

$$f_2^{(4)}(t) = \frac{2}{7}\left(\frac{2\dot{R}^2}{R^2}s_2^2 + \frac{2\dot{R}}{R}s_2\dot{s}_2 - \dot{s}_2^2\right)$$
$$+ \frac{2}{21}\left[8\left(\frac{\ddot{R}}{R} + \frac{2\dot{R}^2}{R^2}\right)s_2 s_4 + 7\ddot{s}_2 s_4 - 3s_2\ddot{s}_4 + \frac{20\dot{R}}{R}(\dot{s}_2 s_4 + s_2\dot{s}_4) + \dot{s}_2\dot{s}_4\right]$$
$$+ \frac{1}{42}\left[\left(\frac{4\ddot{R}}{R} + \frac{23\dot{R}^2}{R^2}\right)s_3^2 + 2s_3\ddot{s}_3 + \frac{35\dot{R}}{R}s_3\dot{s}_3 - \frac{13}{4}\dot{s}_3^2\right]$$
$$+ \frac{8}{693}\left[\left(\frac{10\ddot{R}}{R} + \frac{41\dot{R}^2}{R^2}\right)s_4^2 + 5s_4\ddot{s}_4 + \frac{71\dot{R}}{R}s_4\dot{s}_4 - \dot{s}_4^2\right], \quad (3.8)$$

$$g_2^{(4)}(t) = \frac{9}{14}\left(\frac{6\dot{R}}{R}s_3 u + 4s_3\dot{u} + 5\dot{s}_3 u\right), \quad (3.9)$$

$$f_3^{(4)}(t) = \tfrac{2}{15}\left(\frac{9\dot{R}^2}{R^2} - \frac{\ddot{R}}{R}\right)s_2 s_3 + \tfrac{4}{15}\ddot{s}_2 s_3 + \frac{2\dot{R}}{5R}(\dot{s}_2 s_3 + s_2\dot{s}_3) - \tfrac{3}{5}\dot{s}_2\dot{s}_3 - \tfrac{1}{15}s_2\ddot{s}_3$$
$$+ \tfrac{2}{11}\left(\frac{\ddot{R}}{R} + \frac{7\dot{R}^2}{R^2}\right)s_3 s_4 + \tfrac{3}{11}\ddot{s}_3 s_4 + \frac{10\dot{R}}{11R}(\dot{s}_3 s_4 + s_3\dot{s}_4) - \tfrac{1}{11}\dot{s}_3\dot{s}_4, \quad (3.10)$$

$$g_3^{(4)}(t) = \tfrac{2}{9}\left(\frac{24\dot{R}}{R}s_4 u + 17s_4\dot{u} + 21\dot{s}_4 u\right) - \tfrac{6}{5}\left(\frac{4\dot{R}}{R}s_2 u + s_2\dot{u} + 5\dot{s}_2 u\right), \quad (3.11)$$

$$f_4^{(4)}(t) = -\tfrac{1}{35}\left[16\left(\frac{3\ddot{R}}{R} + \frac{2\dot{R}^2}{R^2}\right)s_2^2 + 6s_2\ddot{s}_2 + \frac{176\dot{R}}{R}s_2\dot{s}_2 + 71\dot{s}_2^2\right]$$
$$+ \tfrac{8}{77}\left[2\left(\frac{6\dot{R}^2}{R^2} - \frac{\ddot{R}}{R}\right)s_2 s_4 + 5\ddot{s}_2 s_4 - s_2\ddot{s}_4 + \frac{3\dot{R}}{R}(\dot{s}_2 s_4 + s_2\dot{s}_4) - 6\dot{s}_2\dot{s}_4\right]$$
$$+ \tfrac{9}{616}\left[4\left(\frac{9\dot{R}^2}{R^2} - \frac{4\ddot{R}}{R}\right)s_3^2 + 8s_3\ddot{s}_3 - \frac{12\dot{R}}{R}s_3\dot{s}_3 - 27\dot{s}_3^2\right]$$
$$+ \tfrac{9}{1001}\left[\frac{8\dot{R}^2}{R^2}s_4^2 + 2s_4\ddot{s}_4 + \frac{8\dot{R}}{R}s_4\dot{s}_4 - \dot{s}_4^2\right], \quad (3.12)$$

$$g_4^{(4)}(t) = -\tfrac{5}{14}\left(\frac{18\dot{R}}{R}s_3 u + 4s_3\dot{u} + 21\dot{s}_3 u\right). \quad (3.13)$$

These equations have been investigated numerically. To make them more suitable for this process, we have incorporated viscous damping of volume oscillations (the last term in brackets on the right-hand side of (3.1)) and supplemented the equation of translation motion with the viscous force in the form of the Levich drag (Levich 1962) (the last term on the right-hand side of (3.2)). The quantity η in the above terms denotes the dynamical viscosity of the liquid.

https://doi.org/10.1017/S0022112003006220 Published online by Cambridge University Press

Before proceeding to numerical calculations, we shall point out some interesting observations which are apparent from (3.1)–(3.13). First, it is worth noting that (3.7) is in complete agreement with the previously established fact, namely, that the translational motion of the bubble can be induced by the second-order interactions of two neighbouring surface modes. Analysis of the other equations allows us to reveal additional features, which have not been noted previously, inherent in the mutual interactions of the shape modes as well as in the interaction between the shape modes and the translational motion. It is easy to see that the translational motion is able to induce oscillations of all other modes even if they are initially nil, the external field is absent and chance fluctuations are negligible. Indeed, the terms proportional to u^2 on the right-hand sides of (3.1) and (3.3) show that the translational motion can excite the volume and quadrupole modes. According to (3.12), the quadrupole mode can, in turn, excite the fourth mode, and (3.11) shows that nonlinear interactions between u and s_2 can also give rise to the third mode. It can be shown that this property of the translational motion is shared by the third mode. The modes s_2 and s_4 do not have this ability. These modes can excite each other and the volume mode but they are unable to excite the third mode and the translational motion if other disturbances are absent. From these facts, it follows that odd modes are more efficient as regards introduction of perturbations into the system and promotion of their evolution.

Numerical solutions of (3.1)–(3.13) have been obtained for the case of air bubbles in water. The values used for hydrostatic pressure, liquid density, surface tension, viscosity, sound speed and specific heat ratio are $P_0 = 1$ bar, $\rho = 998\,\mathrm{kg\,m^{-3}}$, $\sigma = 0.0725\,\mathrm{N\,m^{-1}}$, $\eta = 0.001$ kg ($\mathrm{m^{-1}\ s^{-1}}$), $c = 1500\,\mathrm{m\,s^{-1}}$ and $\gamma = 1.4$.

Figure 1 illustrates the fact that the translational motion of a bubble is able to excite the volume pulsation and the shape modes of all orders even if any other disturbances are absent. In particular, the oscillations shown in figure 1 develop when the initial translational velocity of the bubble $u(0)$ is set equal to $0.2\,\mathrm{m\,s^{-1}}$. Spectrum analysis reveals that the peculiarity of this type of perturbation is that the dominant frequency in the Fourier spectrum of each mode is the natural frequency of that mode. The values of the natural frequencies of the modes are shown in the caption for figure 1. Figure 2 shows oscillations that arise from the disturbance of the second (quadrupole) mode, $s_2(0) = 1\,\mu\mathrm{m}$. In this case, only the even (volume and fourth) modes are excited. Their oscillations are found by spectrum analysis to contain two main frequency components; at the eigenfrequency of the forced mode and at twice the natural frequency of the driving (second) mode, the latter being dominant. In the well-known work of Longuet-Higgins (1989*a*, *b*), it was first pointed out that shape oscillations of bubbles should be accompanied by the excitation of volume pulsations whose frequency is twice the frequency of the shape oscillation. This effect provides a possible mechanism of underwater sound generation in the ocean. In this connection, it is interesting to note that the translational disturbance has the same property, except that the spectrum of the forced volume pulsation in this case is dominated by the natural frequency of the volumetric mode. Comparison of figures 1(*a*) and 2(*a*) gives an idea of the amplitude of this pulsation. Ffowcs Williams & Guo (1991) mention in their paper that in the ocean environment, bubbles usually move, owing to buoyancy or background pressure gradients, with a typical velocity of the order of $0.2\,\mathrm{m\ s^{-1}}$. The volume pulsation in figure 1(*a*) is just generated at this value of the initial translational velocity, all other parameters being the same as in figure 2(*a*). It is seen that the amplitude of the volume pulsation in figure 1(*a*) is less, but not far from the amplitude of the volume pulsation in figure 2(*a*), where the surface distortion

https://doi.org/10.1017/S0022112003006220 Published online by Cambridge University Press

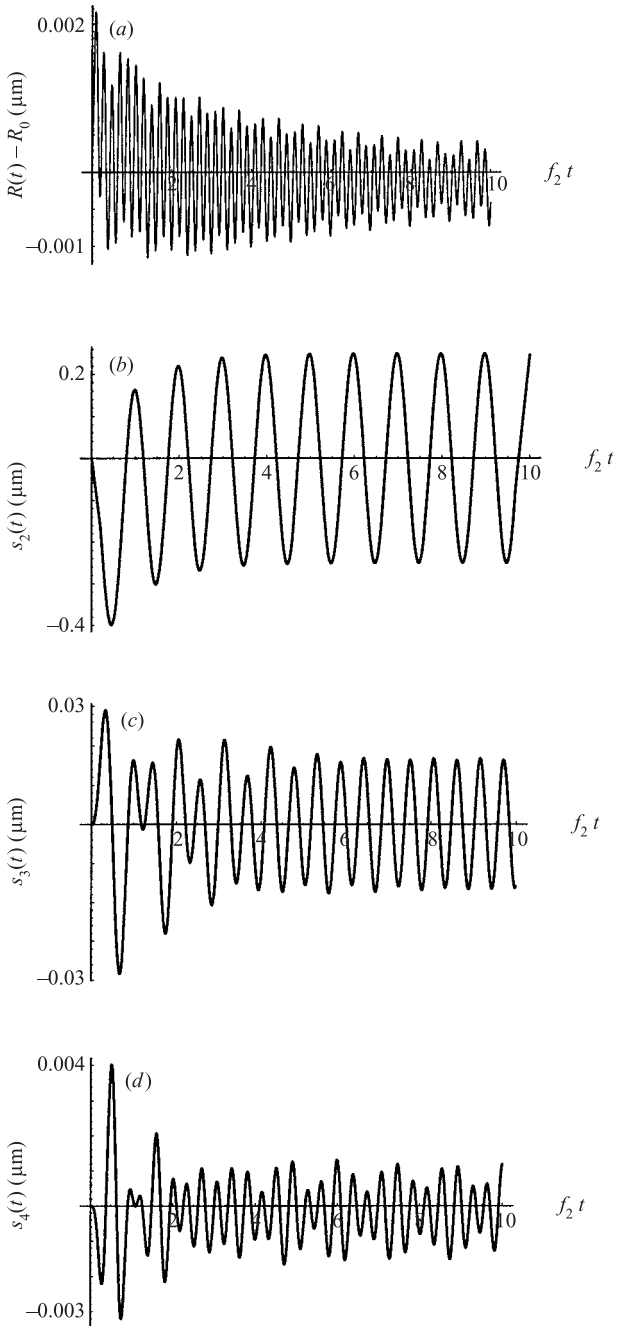


FIGURE 1. The volume and shape oscillations of a bubble ($R_0 = 50\,\mu\text{m}$) resulting from the initial translational perturbation $u(0) = 0.2\,\text{m s}^{-1}$. The natural frequencies of the bubble modes are $f_0 = 66435\,\text{Hz}$, $f_2 = 13291\,\text{Hz}$, $f_3 = 24266\,\text{Hz}$, $f_4 = 36399\,\text{Hz}$.

$s_2(0)$ amounts to 2% of R_0. This suggests that translational disturbances of bubbles also contribute to oceanic ambient noise.

Figure 3 shows oscillations that are generated by the disturbance of the third mode, $s_3(0) = 1\,\mu\text{m}$. Like the translation, the third mode excites all the other modes.

https://doi.org/10.1017/S0022112003006220 Published online by Cambridge University Press

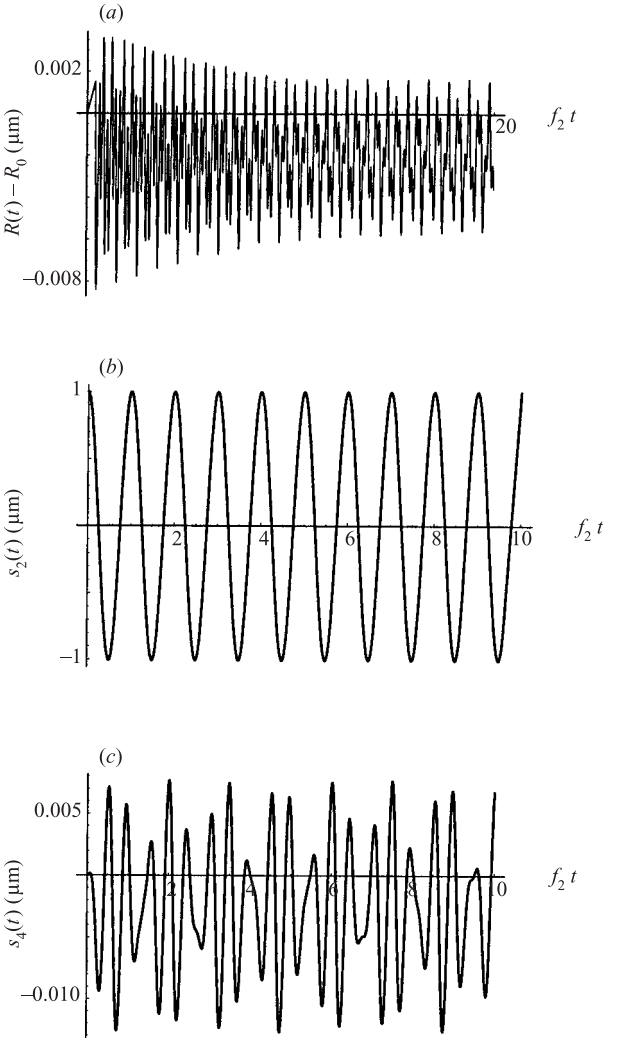


FIGURE 2. The bubble oscillations induced by the initial perturbation of the second mode $s_2(0) = 1$ μm. The other parameters are the same as in figure 1.

The Fourier spectra of the volume, second and fourth modes are found to be of two-component form, like the spectra of the oscillations shown in figures 2(*a*) and 2(*c*), namely, one of the two dominant components is at the eigenfrequency of the forced mode and the other is at twice the natural frequency of the driving (third) mode. The spectrum of the translational oscillation shown in figure 3(*b*), owing to the structure of the function $f_1^{(4)}(t)$, is much richer, see figure 4. It exhibits six main components, including the harmonics with the frequencies f_3 and $3f_3$ which occur because the second and fourth modes have the $2f_3$ components. It may well be that it is the complexity of the translational spectrum that renders this type of motion susceptible to chaotic effects.

Figure 5 demonstrates the initiation of the erratic dancing motion of a bubble in a standing acoustic wave, the bubble being driven below the fundamental resonance. The coefficients A_n, which specify the type of external field in (3.1)–(3.5), were taken

https://doi.org/10.1017/S0022112003006220 Published online by Cambridge University Press

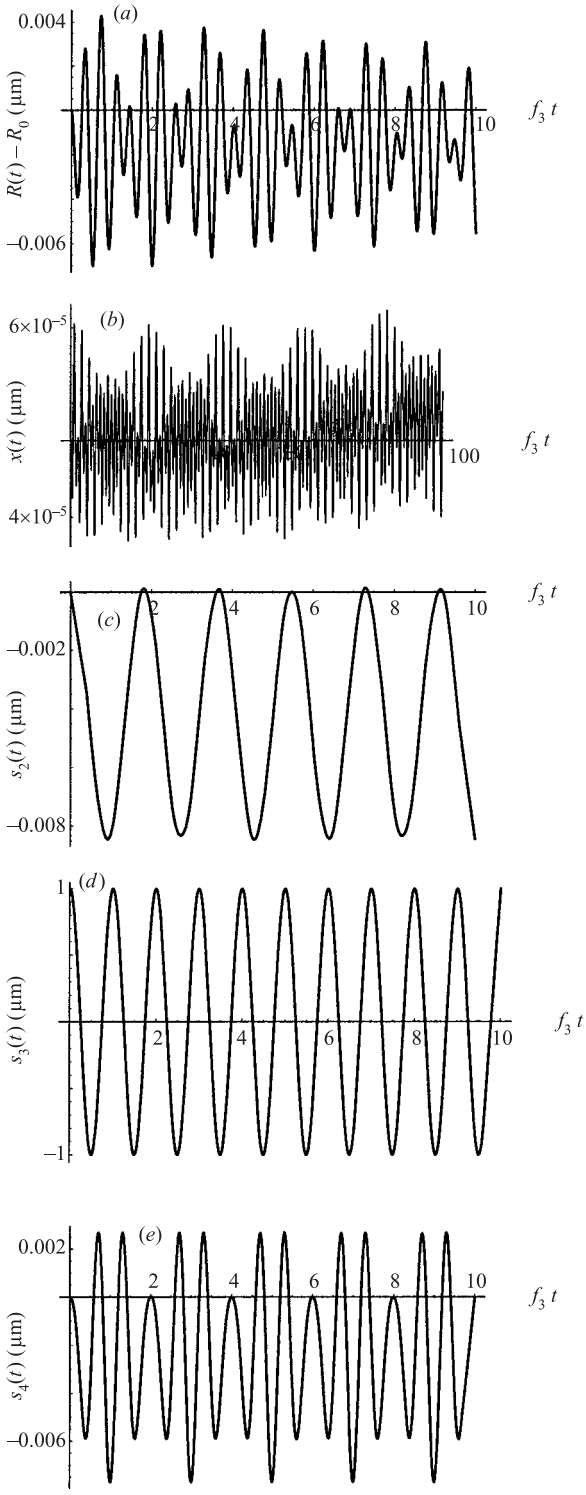


FIGURE 3. The bubble oscillations induced by the initial perturbation of the third mode $s_3(0) = 1\,\mu\text{m}$. The other parameters are the same as in figure 1.

https://doi.org/10.1017/S0022112003006220 Published online by Cambridge University Press

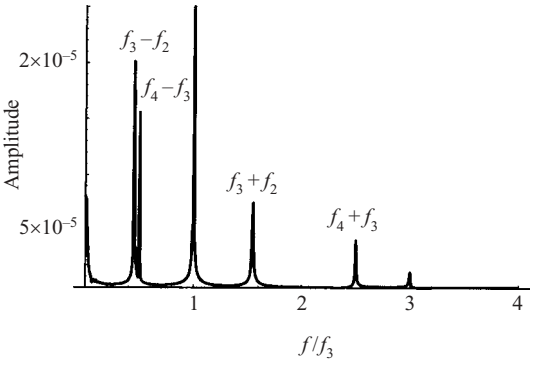


FIGURE 4. Fourier spectrum of the translation shown in figure 3(*b*).

from Appendix A. Figures 5(*a*)–5(*c*) show the evolution of the shape modes. The rapid growth of the unstable third mode can be seen to lead to instability of the second mode, and their nonlinear interaction (sustained also by the interaction of the third and fourth modes) results further in erratic translational motions of the bubble. Evidence of the translational instability first appears in the translational velocity of the bubble, see figure 5(*d*). The motion of the bubble centroid and the onset of the dancing are shown in figure 5(*e*). The position zero of the y-axis on this plot corresponds to the acoustic pressure antinode. On analysis of the bubble natural frequencies, whose values are given in the caption for figure 5, it is easy to verify that in the case under consideration there are no resonances between the forcing and the bubble modes as well as between the modes themselves. This point distinguishes the present case from that investigated by Feng & Leal (1995), where it was assumed that the natural frequencies of the two considered shape modes are approximately half the forcing frequency. Figure 5 demonstrates that even with no resonances, the translational instability can develop very quickly. The case where a bubble is driven above its fundamental resonance is illustrated by figure 6. The dynamics of the bubble centroid are shown in figure 6(*e*). It is seen that the bubble initially moves away from the pressure antinode. However, the development of the translational instability causes it to turn back and make translational jumps about the antinode.

An interesting case of stabilization is shown in figure 7. The acoustic pressure amplitude P_a is here much larger than in the two preceding cases. Therefore the shape oscillations initially develop very vigorously and reach great amplitudes (figure 7*a–c*). This leads to the onset of the dancing motion, figures 7(*d*) and 7(*e*). Then, however, the oscillations of the shape modes decay and become stable. As a result, the dancing motion dies out. An increase of 0.2% in P_a (from $0.44P_0$ to $0.441P_0$), or a change of 1% in the driving frequency f (from 20 kHz to 20.2 kHz or 19.8 kHz), is sufficient for this stabilization to give way to a violent development of instability. Numerical simulations reveal that this effect is caused by the terms $f_n^{(4)}(t)$ and $g_n^{(4)}(t)$ on the right-hand sides of (3.3)–(3.5), in other words, by the nonlinear coupling of the shape modes. If we drop these terms, retaining only the terms $A_n(t)$ (which now play the role of small perturbations for the parametric excitation of the shape modes by the volume pulsation), then we have the shape oscillations shown in figure 8. They are stable as well, but their amplitudes are much smaller than in figure 7. Generally speaking, this case is of considerable interest by itself because we observe

https://doi.org/10.1017/S0022112003006220 Published online by Cambridge University Press

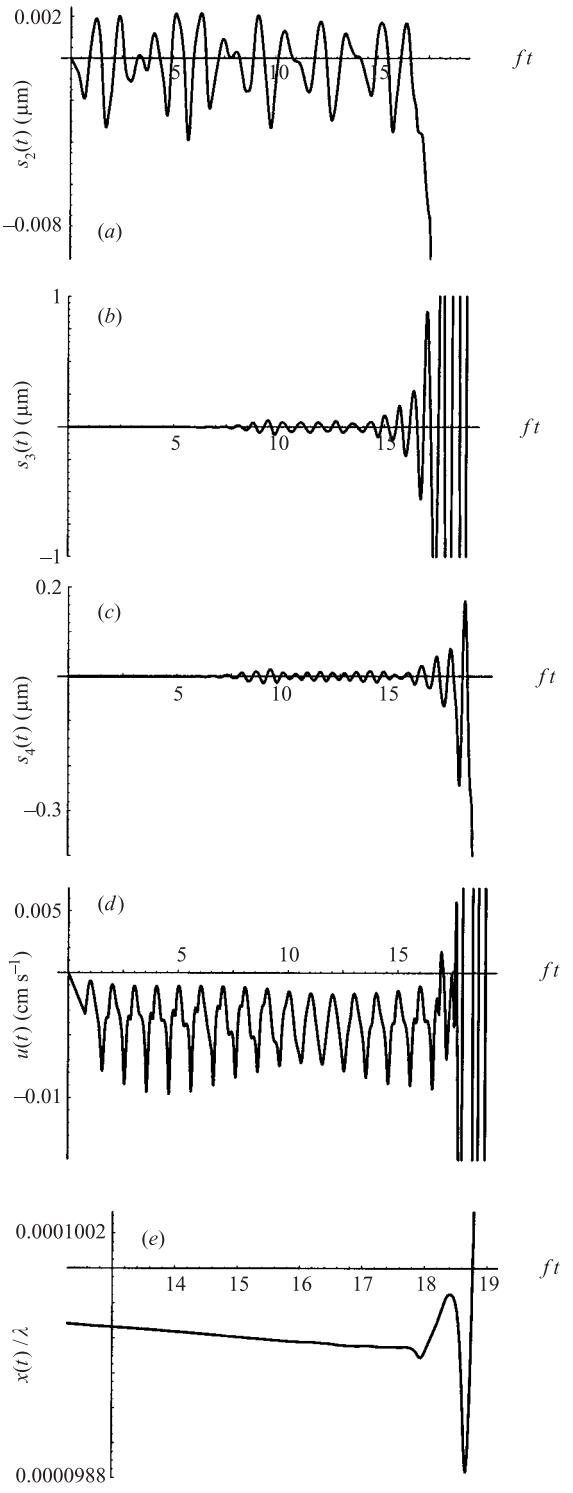


FIGURE 5. Dynamics of a bubble in an acoustic standing wave: driving below resonance ($R_0 = 40\,\mu$m, $f = 28.3$ kHz, $P_a = 0.28P_0$). (*a*) second mode, (*b*) third mode, (*c*) fourth mode, (*d*) translational velocity, (*e*) position of the bubble centroid ($\lambda = c/f$). The natural bubble frequencies are $f_0 = 83266$ Hz, $f_2 = 18575$ Hz, $f_3 = 33913$ Hz, $f_4 = 50869$ Hz.

https://doi.org/10.1017/S0022112003006220 Published online by Cambridge University Press

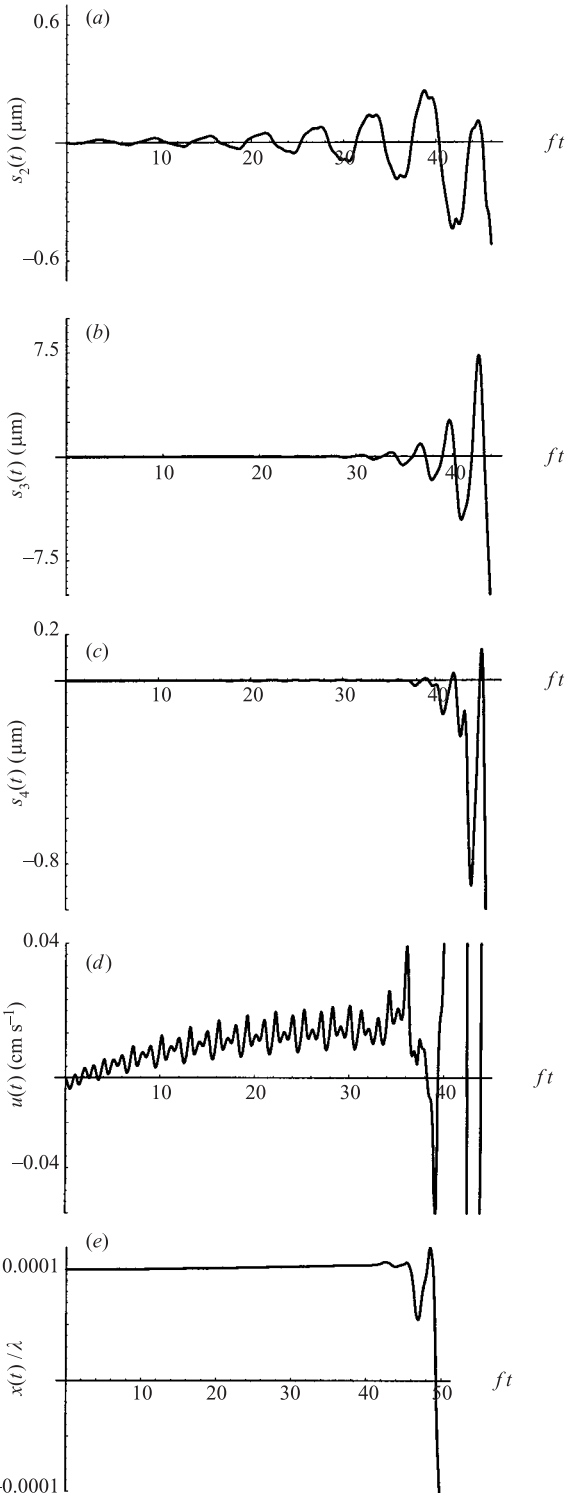


FIGURE 6. Dynamics of a bubble in an acoustic standing wave: Driving above resonance ($R_0 = 50\,\mu$m, $f = 100$ kHz, $P_a = 0.35P_0$). (*a*) second mode, (*b*) third mode, (*c*) fourth mode, (*d*) translational velocity, (*e*) position of the bubble centroid ($\lambda = c/f$). The natural bubble frequencies are $f_0 = 66435$ Hz, $f_2 = 13291$ Hz, $f_3 = 24266$ Hz, $f_4 = 36399$ Hz.

https://doi.org/10.1017/S0022112003006220 Published online by Cambridge University Press

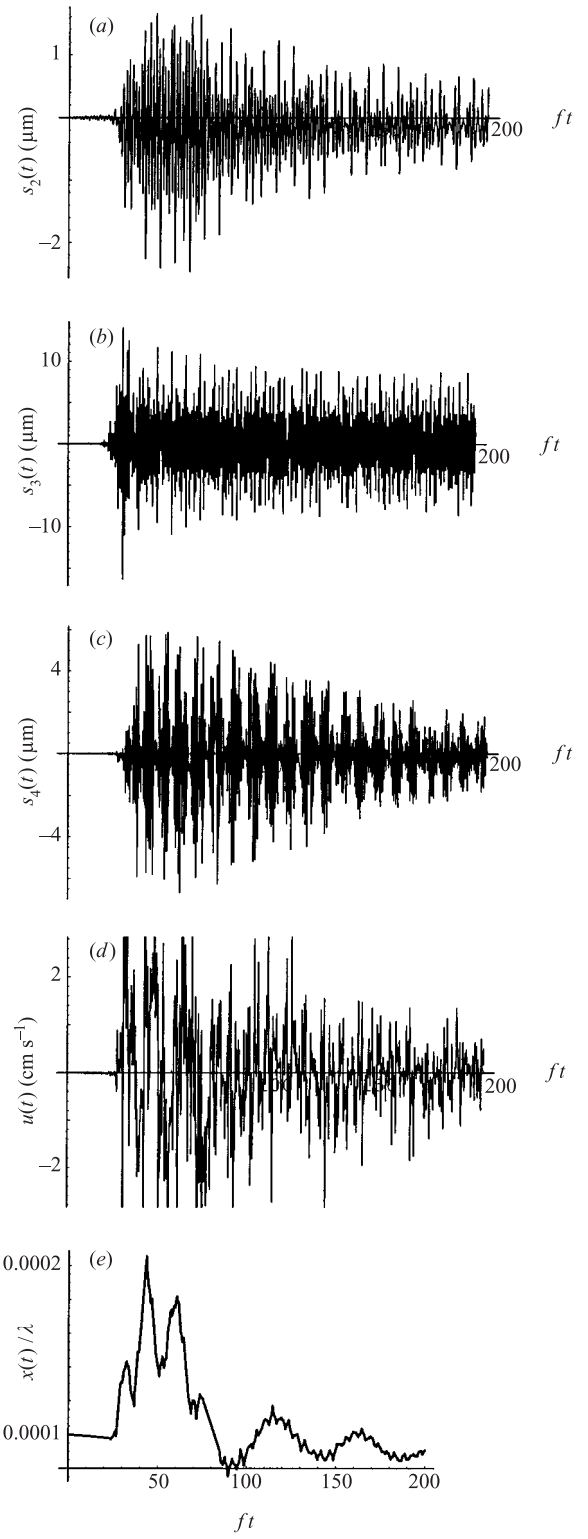


FIGURE 7. Dynamics of a bubble in an acoustic standing wave: example of stabilization ($R_0 = 50\,\mu\text{m}$, $f = 20\,\text{kHz}$, $P_a = 0.44P_0$). The natural bubble frequencies are the same as in figure 6.

https://doi.org/10.1017/S0022112003006220 Published online by Cambridge University Press

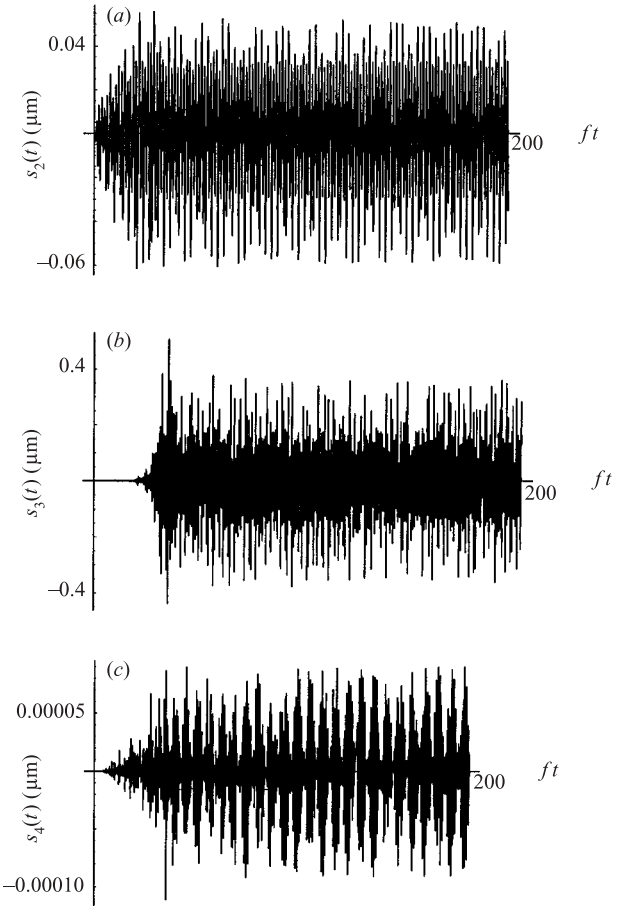


FIGURE 8. The same case as in figure 7 but dropping the terms $f_n^{(4)}(t)$ and $g_n^{(4)}(t)$ on the right-hand sides of (3.3)–(3.5).

stable shape oscillations of quite a large bubble ($R_0 = 50\,\mu$m) in a fairly strong field ($P_a = 0.44P_0$). Calculations show that if the driving frequency is changed from 20 kHz to 20.5 kHz (or P_a to $0.446P_0$), the oscillations in figure 8 become unstable. The dependence of the stability of shape oscillations on values of the driving frequency is, however, poorly elucidated in the literature. Therefore, it is hard to tell now why this occurs for the present set of parameters. Turning back to comparison of figures 7 and 8, we can conclude that the nonlinear coupling between the shape modes leads to a great increase in their starting amplitudes. However, shortly thereafter, owing to the same coupling, the shape oscillations decay, and the system becomes stable again.

4. Comparison with Feng & Leal (1995)

Numerical examples given by Feng & Leal (1995) refer to the interaction of the fifth and sixth shape modes. To carry out analogous calculations, (2.23)–(2.27) should be taken with accuracy up to mode s_6. As a result, (3.1)–(3.5) are supplemented

https://doi.org/10.1017/S0022112003006220 Published online by Cambridge University Press

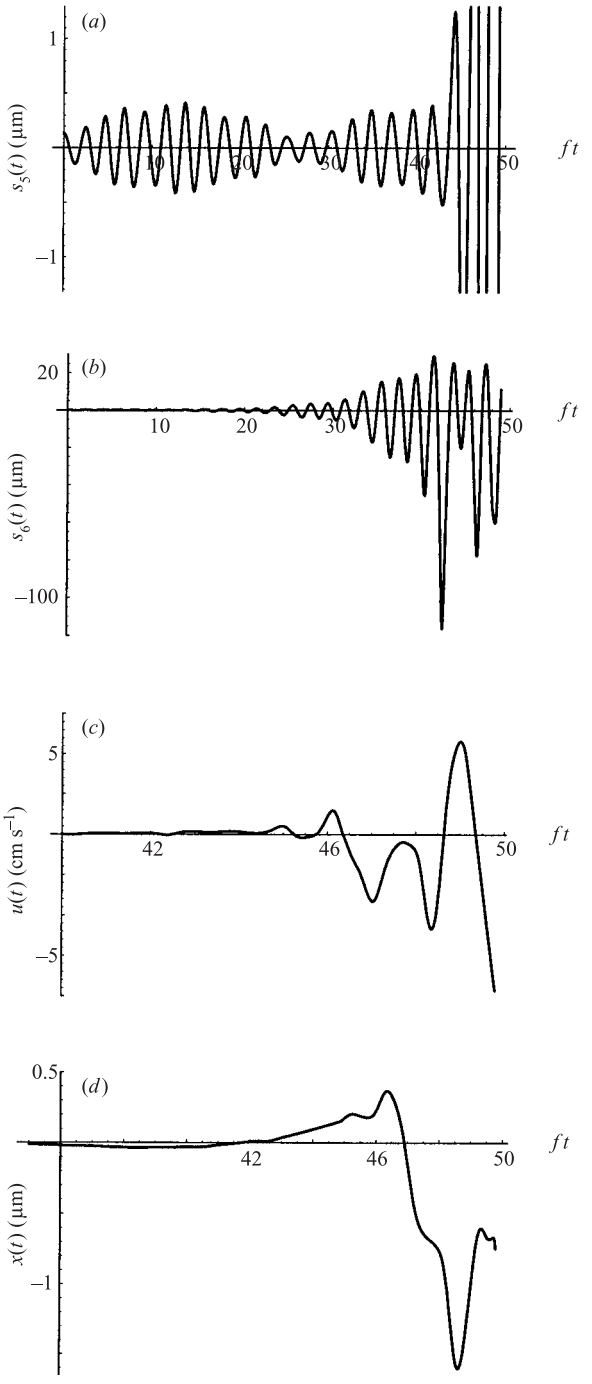


FIGURE 9. Translational motion of a bubble due to the interaction of the fifth and sixth shape modes which evolve from radial oscillation via a parametric instability. Initial perturbations of the other modes are zero.

https://doi.org/10.1017/S0022112003006220 Published online by Cambridge University Press

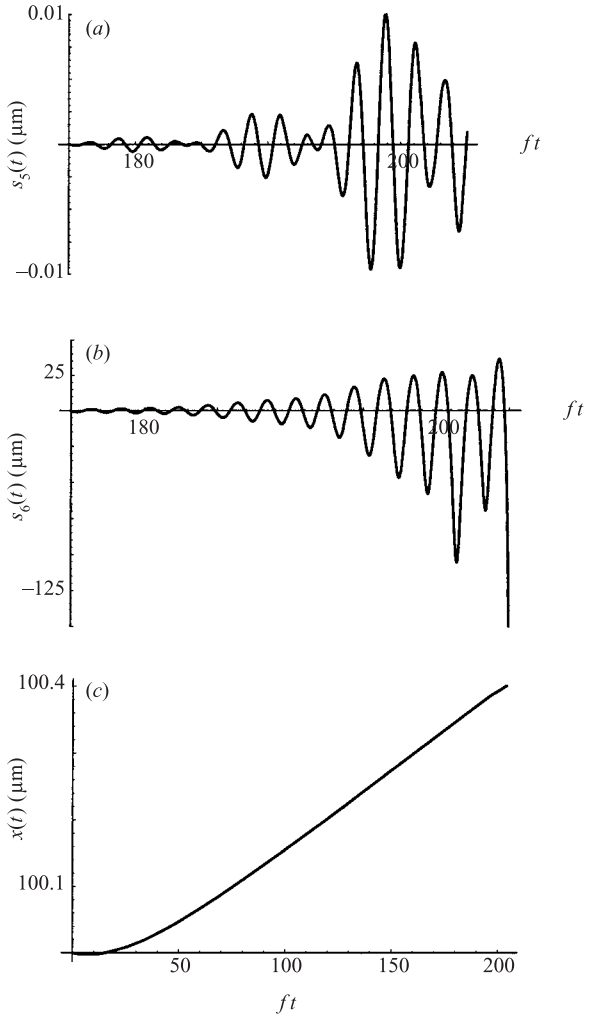


FIGURE 10. The bubble is driven by a plane standing acoustic wave. The other parameters are the same as in figure 9.

with two equations

$$R\ddot{s}_5 + 3\dot{R}\dot{s}_5 + \left(\frac{168\sigma}{\rho R^2} - 4\ddot{R}\right)s_5 = -\frac{6}{\rho}A_5 + f_5^{(6)}(t) + g_5^{(6)}(t), \tag{4.1}$$

$$R\ddot{s}_6 + 3\dot{R}\dot{s}_6 + \left(\frac{280\sigma}{\rho R^2} - 5\ddot{R}\right)s_6 = -\frac{7}{\rho}A_6 + f_6^{(6)}(t) + g_6^{(6)}(t), \tag{4.2}$$

and the functions $f_n^{(4)}(t)$ and $g_n^{(4)}(t)$ on their right-hand sides are replaced with $f_n^{(6)}(t)$ and $g_n^{(6)}(t)$, which, along with the similar functions appearing in (4.1) and (4.2), are given in Appendix B.†

† Appendix B is available as a supplement to the online version of this paper, or from the author or JFM Editorial Office, Cambridge.

https://doi.org/10.1017/S0022112003006220 Published online by Cambridge University Press

Feng & Leal used non-dimensional parameters. Converting them to dimensional values and applying them to an air bubble in water, for figure 6 of their paper, we obtain $R_0 = 138\,\mu\text{m}$, $f = 26716\,\text{Hz}$ and $P_a = 0.016$ bar. We used the same values for R_0 and f, and a slightly lower value for P_a. Our approach, unlike Feng & Leal's, does not allow for viscous damping of shape modes. Therefore, their growth occurs faster. To slow down this process and extend the interval of observation, we set $P_a = 0.013$ bar. Feng & Leal assumed that the fifth and sixth modes are parametrically excited by the spherical volume mode that is forced by an isotropic pressure oscillation at infinity. Modelling the same situation, we set $p_{ex}(t) = -P_a \sin \omega t$ and $s_5(0) = s_6(0) = 0.001 R_0$, while initial perturbations of the other modes are zero. The results of the simulation are presented in figure 9. We see that, just as in Feng & Leal (1995), the instability of the sixth mode, figure 9(*b*), leads to instability of the fifth mode, figure 9(*a*), which is otherwise stable. The instability of these two neighbouring shape modes results in a translational motion of the bubble (figure 9*c*, *d*). We can also see from figure 9(*b*) that, as in Feng & Leal (1995), the onset of the erratic translation damps out the oscillation of the sixth mode.

Figure 10 illustrates the case where the same bubble is driven by a plane standing acoustic wave with the same values of f and P_a as in figure 9. In other words, all the bubble modes are now subjected to perturbations, which are specified by the coefficients $A_n(t)$. The bubble is to the right of the pressure antinode in the direction of wave propagation at an initial distance of $100\,\mu\text{m}$. We can see that, although the amplitude of the unstable sixth mode runs up to high values, the translational instability is not observed. It appears to be lost against the background of the translational motion caused by the primary Bjerknes force. Besides, a relatively small initial perturbation of the fifth mode does not allow the latter to develop adequately and thereby the performance of its interaction with the sixth mode is reduced. As a consequence, the bubble moves towards the pressure node without any visible jumps. This result, especially when compared to figures 5 and 6, seems to suggest that the influence of shape modes of high order on translational motions of bubbles in real (anisotropic) acoustic fields is in general weak and hence the case considered by Feng & Leal is of academic interest rather than of practical importance.

5. Conclusion

A set of coupled equations has been derived that governs volume pulsations of a bubble, its translational motion and shape oscillations evolving on the bubble surface. Using a perturbation analysis, where the amplitudes of the shape modes and the translational velocity of the bubble are assumed to be small parameters, the equations of the bubble motions are obtained with accuracy up to quadratic terms in those quantities. The equations obtained allow us to study the translational instability of an acoustically driven bubble that is known as 'dancing motion'. Unlike earlier work on this subject, where only two adjacent shape modes with given natural frequencies are taken into account, we allow for all shape modes and do not impose any limitations on their natural frequencies. As a result, the present analysis reveals additional features, which have not been noted previously, inherent in the mutual interactions of the shape modes as well as in the interaction between the shape modes and the translational motion. In particular, it is shown that an odd shape mode and the translational motion can excite all other modes, including the volume mode, even if they are initially nil, the external field is absent and chance fluctuations are negligible. Even shape modes do not have this ability. They can only excite each

https://doi.org/10.1017/S0022112003006220 Published online by Cambridge University Press

other and the volume mode. Thus, it is apparent that odd modes are more important as regards introduction of perturbations into the system and promotion of their evolution. It is also noted that translational disturbances of bubbles, as they are able to excite volume pulsations, can contribute to oceanic ambient noise parallel with the known shape-mode mechanism. It is shown that the translational instability of an acoustically driven bubble can develop very quickly even if there are no resonances between the forcing and the bubble modes as well as between the modes themselves. This feature distinguishes the present analysis from all previous studies where specific resonant cases are only considered.

Appendix A. Coefficients $A_n(t)$ in a plane standing wave

In the case of a plane standing wave, the acoustic pressure at an arbitrary point of the host liquid can be written as

$$p_{ex} = -P_a \sin\omega t \cos(kz + \boldsymbol{k}\cdot\boldsymbol{r}), \tag{A 1}$$

where P_a is the pressure amplitude, ω the angular driving frequency, k the wavenumber in the host liquid, $z(t)$ the location of the bubble centroid with respect to the nearest pressure antinode, and $\boldsymbol{r}$ the position vector whose origin coincides with the bubble centroid. Using the well-known expansion (Abramowitz & Stegun 1972)

$$\exp(\mathrm{i}kr\mu) = \sum_{n=0}^{\infty} (2n+1) i^n j_n(kr) P_n(\mu), \tag{A 2}$$

where j_n denotes the spherical Bessel function of order n, we find

$$\cos(kz + \boldsymbol{k}\cdot\boldsymbol{r}) = \tfrac{1}{2}\sum_{n=0}^{\infty} (2n+1) i^n j_n(kr)[\exp(\mathrm{i}kz) + (-1)^n \exp(-\mathrm{i}kz)] P_n(\mu). \tag{A 3}$$

Substituting (A 3) into (A 1), setting $r = R(t)$ and comparing with (2.21), we obtain

$$A_n(t) = -\tfrac{1}{2}(2n+1) i^n j_n(kR)[\exp(\mathrm{i}kz) + (-1)^n \exp(-\mathrm{i}kz)] P_a \sin\omega t. \tag{A 4}$$

Appendix B. Expressions for the functions $f_n(t)$ and $g_n(t)$ accurate to the sixth mode

When (2.26) and (2.27) are taken with accuracy up to the sixth shape mode s_6, we obtain

$$f_0^{(6)}(t) = f_0^{(4)}(t) - \frac{3\gamma P_{g0} R_0^{3\gamma}}{\rho R^{3\gamma+2}}\left(\frac{s_5^2}{11} + \frac{s_6^2}{13}\right) + \frac{1}{132}\left[\frac{20\dot{R}}{R}\left(\frac{\dot{R}}{R}s_5 + \dot{s}_5\right)s_5 - 12 s_5\ddot{s}_5 - 13\dot{s}_5^2\right]$$
$$+ \frac{1}{182}\left[\frac{24\dot{R}}{R}\left(\frac{\dot{R}}{R}s_6 + \dot{s}_6\right)s_6 - 14 s_6\ddot{s}_6 - 15\dot{s}_6^2\right],$$

$$f_1^{(6)}(t) = f_1^{(4)}(t) + \frac{1}{33}\left[8\left(\frac{\ddot{R}}{R} + \frac{3\dot{R}^2}{R^2}\right)s_4 s_5 + 4\ddot{s}_4 s_5 - 5 s_4\ddot{s}_5 + \frac{24\dot{R}}{R}(\dot{s}_4 s_5 + s_4\dot{s}_5) - 3\dot{s}_4\dot{s}_5\right]$$
$$+ \frac{3}{143}\left[10\left(\frac{\ddot{R}}{R} + \frac{3\dot{R}^2}{R^2}\right)s_5 s_6 + 5\ddot{s}_5 s_6 - 6 s_5\ddot{s}_6 + \frac{30\dot{R}}{R}(\dot{s}_5 s_6 + s_5\dot{s}_6) - 3\dot{s}_5\dot{s}_6\right],$$

https://doi.org/10.1017/S0022112003006220 Published online by Cambridge University Press

$$f_2^{(6)}(t) = f_2^{(4)}(t) + \frac{25}{77}\left[2\left(\frac{\ddot{R}}{R} + \frac{2\dot{R}^2}{R^2}\right)s_3s_5 + \tfrac{5}{3}\ddot{s}_3s_5 - \tfrac{2}{3}s_3\ddot{s}_5 + \frac{5\dot{R}}{R}(\dot{s}_3s_5 + s_3\dot{s}_5) + \tfrac{1}{2}\dot{s}_3\dot{s}_5\right]$$
$$+ \frac{5}{143}\left[16\left(\frac{\ddot{R}}{R} + \frac{2\dot{R}^2}{R^2}\right)s_4s_6 + 13\ddot{s}_4s_6 - 5s_4\ddot{s}_6 + \frac{40\dot{R}}{R}(\dot{s}_4s_6 + s_4\dot{s}_6) + 5\dot{s}_4\dot{s}_6\right]$$
$$+ \frac{25}{429}\left[\left(\frac{2\ddot{R}}{R} + \frac{7\dot{R}^2}{R^2}\right)s_5^2 + \ddot{s}_5s_5 + \frac{13\dot{R}}{R}\dot{s}_5s_5 + \tfrac{1}{4}\dot{s}_5^2\right]$$
$$+ \frac{2}{1001}\left[2\left(\frac{28\ddot{R}}{R} + \frac{89\dot{R}^2}{R^2}\right)s_6^2 + 28\ddot{s}_6s_6 + \frac{346\dot{R}}{R}\dot{s}_6s_6 + 13\dot{s}_6^2\right],$$

$$g_2^{(6)}(t) = g_2^{(4)}(t),$$

$$f_3^{(6)}(t) = f_3^{(4)}(t) + \frac{40}{99}\left(\frac{3\ddot{R}}{R} + \frac{5\dot{R}^2}{R^2}\right)s_2s_5 + \tfrac{10}{33}(4\ddot{s}_2s_5 - s_2\ddot{s}_5) + \frac{280\dot{R}}{99R}(\dot{s}_2s_5 + s_2\dot{s}_5)$$
$$+ \tfrac{50}{99}\dot{s}_2\dot{s}_5 + \frac{50}{143}\left(\frac{3\ddot{R}}{R} + \frac{5\dot{R}^2}{R^2}\right)s_3s_6 + \tfrac{25}{429}(17\ddot{s}_3s_6 - 4s_3\ddot{s}_6) + \frac{350\dot{R}}{143R}(\dot{s}_3s_6 + s_3\dot{s}_6)$$
$$+ \tfrac{75}{143}\dot{s}_3\dot{s}_6 + \frac{4}{429}\left(\frac{29\ddot{R}}{R} + \frac{123\dot{R}^2}{R^2}\right)s_4s_5 + \tfrac{2}{429}(54\ddot{s}_4s_5 + 5s_4\ddot{s}_5)$$
$$+ \frac{140\dot{R}}{143R}(\dot{s}_4s_5 + s_4\dot{s}_5) + \tfrac{10}{143}\dot{s}_4\dot{s}_5 + \frac{14}{429}\left(\frac{9\ddot{R}}{R} + \frac{31\dot{R}^2}{R^2}\right)s_5s_6$$
$$+ \tfrac{2}{429}(49\ddot{s}_5s_6 + 7s_5\ddot{s}_6) + \frac{406\dot{R}}{429R}(\dot{s}_5s_6 + s_5\dot{s}_6) + \tfrac{56}{429}\dot{s}_5\dot{s}_6,$$

$$g_3^{(6)}(t) = g_3^{(4)}(t),$$

$$f_4^{(6)}(t) = f_4^{(4)}(t) + \frac{120}{143}\left(\frac{2\ddot{R}}{R} + \frac{3\dot{R}^2}{R^2}\right)s_2s_6 + \tfrac{15}{143}(17\ddot{s}_2s_6 - 3s_2\ddot{s}_6)$$
$$+ \frac{540\dot{R}}{143R}(\dot{s}_2s_6 + s_2\dot{s}_6) + \tfrac{135}{143}\dot{s}_2\dot{s}_6 + \frac{30}{1001}\left(\frac{7\ddot{R}}{R} + \frac{48\dot{R}^2}{R^2}\right)s_3s_5$$
$$+ \tfrac{15}{1001}(33\ddot{s}_3s_5 - 2s_3\ddot{s}_5) + \frac{1035\dot{R}}{1001R}(\dot{s}_3s_5 + s_3\dot{s}_5) - \tfrac{45}{2002}\dot{s}_3\dot{s}_5$$
$$+ \frac{48}{143}\left(\frac{\ddot{R}}{R} + \frac{4\dot{R}^2}{R^2}\right)s_4s_6 + \tfrac{64}{143}\ddot{s}_4s_6 + \frac{168\dot{R}}{143R}(\dot{s}_4s_6 + s_4\dot{s}_6) + \tfrac{24}{143}\dot{s}_4\dot{s}_6$$
$$+ \frac{4}{143}\left(\frac{3\ddot{R}}{R} + \frac{22\dot{R}^2}{R^2}\right)s_5^2 + \tfrac{24}{143}\ddot{s}_5s_5 + \frac{124\dot{R}}{143R}\dot{s}_5s_5 + \tfrac{4}{143}\dot{s}_5^2$$
$$+ \frac{288}{17017}\left(\frac{7\ddot{R}}{R} + \frac{33\dot{R}^2}{R^2}\right)s_6^2 + \frac{36}{221}\ddot{s}_6s_6 + \frac{15552\dot{R}}{17017R}\dot{s}_6s_6 + \frac{1242}{17017}\dot{s}_6^2,$$

$$g_4^{(6)}(t) = g_4^{(4)}(t) + \frac{5}{22}\left(\frac{30\dot{R}}{R}s_5u + 22s_5\dot{u} + 27\dot{s}_5u\right),$$

$$f_5^{(6)}(t) = -\frac{10}{21}\left(\frac{7\ddot{R}}{R} + \frac{5\dot{R}^2}{R^2}\right)s_2s_3 - \frac{5}{21}s_2\ddot{s}_3 - \frac{130\dot{R}}{21R}(\dot{s}_2s_3 + s_2\dot{s}_3) - \tfrac{95}{21}\dot{s}_2\dot{s}_3$$
$$+ \frac{10}{39}\left(\frac{5\dot{R}^2}{R^2} - \frac{\ddot{R}}{R}\right)s_2s_5 + \tfrac{5}{39}(6\ddot{s}_2s_5 - s_2\ddot{s}_5) + \frac{10\dot{R}}{39R}(\dot{s}_2s_5 + s_2\dot{s}_5) - \tfrac{25}{39}\dot{s}_2\dot{s}_5$$

https://doi.org/10.1017/S0022112003006220 Published online by Cambridge University Press

$$+\frac{2}{91}\left(\frac{43\dot{R}^2}{R^2}-\frac{31\ddot{R}}{R}\right)s_3s_4+\tfrac{1}{91}(25\ddot{s}_3s_4+4s_3\ddot{s}_4)-\frac{50\dot{R}}{91R}(\dot{s}_3s_4+s_3\dot{s}_4)-\tfrac{85}{91}\dot{s}_3\dot{s}_4$$
$$+\frac{2}{1911}\left(\frac{1495\dot{R}^2}{R^2}-\frac{19\ddot{R}}{R}\right)s_3s_6+\tfrac{2}{1911}(602\ddot{s}_3s_6-97s_3\ddot{s}_6)$$
$$+\frac{1438\dot{R}}{1911R}(\dot{s}_3s_6+s_3\dot{s}_6)-\tfrac{310}{1911}\dot{s}_3\dot{s}_6+\frac{4}{39}\left(\frac{13\dot{R}^2}{R^2}-\frac{\ddot{R}}{R}\right)s_4s_5+\tfrac{4}{39}(3\ddot{s}_4s_5+s_4\ddot{s}_5)$$
$$+\frac{20\dot{R}}{39R}(\dot{s}_4s_5+s_4\dot{s}_5)+\tfrac{64}{39}\dot{s}_4\dot{s}_5+\tfrac{80}{663}\left(\frac{11\dot{R}^2}{R^2}+\frac{\ddot{R}}{R}\right)s_5s_6+\tfrac{40}{663}(5\ddot{s}_5s_6+2s_5\ddot{s}_6)$$
$$+\frac{560\dot{R}}{663R}(\dot{s}_5s_6+s_5\dot{s}_6)+\tfrac{40}{663}\dot{s}_5\dot{s}_6,$$

$$g_5^{(6)}(t)=\frac{9}{13}\left(\frac{12\dot{R}}{R}s_6u+9s_6\dot{u}+11\dot{s}_6u\right)-\frac{1}{3}\left(\frac{24\dot{R}}{R}s_4u+5s_4\dot{u}+27\dot{s}_4u\right),$$

$$f_6^{(6)}(t)=-\frac{16}{33}\left(\frac{8\ddot{R}}{R}+\frac{3\dot{R}^2}{R^2}\right)s_2s_4+\tfrac{1}{33}(5\ddot{s}_2s_4-9s_2\ddot{s}_4)-\frac{80\dot{R}}{11R}(\dot{s}_2s_4+s_2\dot{s}_4)-5\dot{s}_2\dot{s}_4$$
$$+\frac{8}{55}\left(\frac{9\dot{R}^2}{R^2}-\frac{2\ddot{R}}{R}\right)s_2s_6+\tfrac{8}{55}(7\ddot{s}_2s_6-s_2\ddot{s}_6)+\frac{12\dot{R}}{55R}(\dot{s}_2s_6+s_2\dot{s}_6)-\tfrac{36}{55}\dot{s}_2\dot{s}_6$$
$$-\frac{75}{154}\left(\frac{3\dot{R}^2}{R^2}+\frac{4\ddot{R}}{R}\right)s_3^2-\tfrac{25}{231}\ddot{s}_3s_3-\frac{1125\dot{R}}{154R}\dot{s}_3s_3-\tfrac{1525}{616}s_3^2$$
$$+\frac{28}{33}\left(\frac{\dot{R}^2}{R^2}-\frac{\ddot{R}}{R}\right)s_3s_5+\tfrac{14}{33}\ddot{s}_3s_5-\frac{28\dot{R}}{33R}(\dot{s}_3s_5+s_3\dot{s}_5)-\tfrac{35}{33}\dot{s}_3\dot{s}_5$$
$$+\frac{8}{33}\left(\frac{23\dot{R}^2}{15R^2}-\frac{2\ddot{R}}{R}\right)s_4^2+\tfrac{16}{99}\ddot{s}_4s_4-\frac{536\dot{R}}{495R}\dot{s}_4s_4-\tfrac{284}{495}\dot{s}_4^2$$
$$+\frac{32}{187}\left(\frac{8\dot{R}^2}{R^2}-\frac{\ddot{R}}{R}\right)s_4s_6+\tfrac{12}{187}(7\ddot{s}_4s_6+s_4\ddot{s}_6)+\frac{80\dot{R}}{187R}(\dot{s}_4s_6+s_4\dot{s}_6)-\tfrac{4}{17}\dot{s}_4\dot{s}_6$$
$$+\frac{40}{561}\left(\frac{9\dot{R}^2}{R^2}-\frac{2\ddot{R}}{R}\right)s_5^2+\tfrac{40}{187}\ddot{s}_5s_5+\frac{40\dot{R}}{187R}\dot{s}_5s_5-\tfrac{30}{187}\dot{s}_5^2$$
$$+\frac{200}{174097}\left[12\left(\frac{256\dot{R}^2}{R^2}-\frac{27\ddot{R}}{R}\right)s_6^2-218\ddot{s}_6s_6-4380\frac{\dot{R}}{R}\dot{s}_6s_6-1863\dot{s}_6^2\right],$$

$$g_6^{(6)}(t)=-\frac{21}{22}\left(\frac{10\dot{R}}{R}s_5u+2s_5\dot{u}+11\dot{s}_5u\right).$$

REFERENCES

Abramowitz, M. & Stegun, I. A. 1972 *Handbook of Mathematical Functions*. Dover.

Benjamin, T. B. 1964 Surface effects in non-spherical motions of small cavities. In *Cavitation in Real Liquids* (ed. R. Davies), pp. 164–180. Elsevier.

Benjamin, T. B. 1987 Hamiltonian theory for motions of bubbles in an infinite liquid. *J. Fluid Mech.* **181**, 349–379.

Benjamin, T. B. & Ellis, A. T. 1990 Self-propulsion of asymmetrically vibrating bubbles. *J. Fluid Mech.* **212**, 65–80.

Benjamin, T. B. & Strasberg, M. 1958 Excitation of oscillations in the shape of pulsating gas bubbles; theoretical work (abstract). *J. Acoust. Soc. Am.* **30**, 697.

https://doi.org/10.1017/S0022112003006220 Published online by Cambridge University Press

Eller, A. 1968 Force on a bubble in a standing acoustic wave. *J. Acoust. Soc. Am.* **43**, 170–171.

Eller, A. I. & Crum, L. A. 1970 Instability of the motion of a pulsating bubble in a sound field. *J. Acoust. Soc. Am.* **47**, 762–767.

Feng, Z. C. & Leal, L. G. 1995 Translational instability of a bubble undergoing shape oscillations. *Phys. Fluids* **7**, 1325–1336.

Ffowcs Williams, J. E. & Guo, Y. P. 1991 On resonant nonlinear bubble oscillations. *J. Fluid Mech.* **224**, 507–529.

Gaines, N. 1932 Magnetostriction oscillator producing intense audible sound and some effects obtained. *Physics* **3**, 209–229.

Harkin, A., Kaper, T. J. & Nadim, A. 2001 Coupled pulsation and translation of two gas bubbles in a liquid. *J. Fluid Mech.* **445**, 377–411.

Kornfeld, M. & Suvorov, L. 1944 On the destructive action of cavitation. *J. Appl. Phys.* **15**, 495–506.

Kuznetsov, G. N. & Shchekin, I. E. 1973 Interaction of pulsating bubbles in a viscous fluid. *Sov. Phys. Acoust.* **18**, 466–469.

Levich, B. V. 1962 *Physicochemical Hydrodynamics.* Prentice-Hall.

Longuet-Higgins, M. S. 1989*a* Monopole emission of sound by asymmetric bubble oscillations. Part 1. Normal modes. *J. Fluid Mech.* **201**, 525–541.

Longuet-Higgins, M. S. 1989*b* Monopole emission of sound by asymmetric bubble oscillations. Part 2. An initial-value problem. *J. Fluid Mech.* **201**, 543–565.

Mei, C. C. & Zhou, X. 1991 Parametric resonance of a spherical bubble. *J. Fluid Mech.* **229**, 29–50.

Prosperetti, A. 1977 Viscous effects on perturbed spherical flows. *Q. Appl. Math.* **34**, 339–352.

Strasberg, M. & Benjamin, T. B. 1958 Excitation of oscillations in the shape of pulsating gas bubbles; experimental work (abstract). *J. Acoust. Soc. Am.* **30**, 697.

Varshalovich, D. A., Moskalev, A. N. & Khersonskii, V. K. 1975 *Quantum Theory of Angular Momentum.* Nauka.

https://doi.org/10.1017/S0022112003006220 Published online by Cambridge University Press